

https://doi.org/10.1070/QEL17434

Thermal optical properties, *Q*-switching and frequency tuning of an Nd:LGGG laser based on the $^4F_{3/2} \rightarrow {}^4I_{13/2}$ transition of a neodymium ion

Shang Gao, Wei Wang

Abstract. **Laser characteristics of continuous-wave (cw) and passively *Q*-switched Nd:LGGG lasers based on the $^4F_{3/2} \rightarrow {}^4I_{13/2}$ transition of an neodymium ion are investigated. The lasing spectra of the cw and the *Q*-switching regimes are studied in detail. The thermal optical coefficient for the Nd:LGGG crystal at a wavelength of 1.33 μm is estimated to be 15.3×10^{-6} K^{-1}. By inserting a quartz plate at the Brewster angle, the frequency of the Nd:LGGG laser is tuned. In the cw regime, the maximum output power at an incident pump power of 7.09 W is 802 mW and a slope efficiency is 13.2%. In the *Q*-switching regime, a minimum pulse duration of 9.75 ns is obtained with an output power of 176 mW and a repetition rate of 8 kHz. The maximum pulse energy and the highest peak power are 25.4 μJ and 2.4 kW, respectively.**

Keywords: *Q-switching, Nd:LGGG disordered crystal, tunable laser.*

1. Introduction

Due to the advantages of simplicity, high-efficiency and low-cost, diode-pumped solid-state lasers have attracted a lot of attention. These lasers operating at 1.3 μm find many applications in the fields of spectroscopy, micro machining, optical communication and remote sensing. Furthermore, harmonic conversions of 1.3 μm can be used in display, laser therapeutics and biomedical applications. Neodymium-doped crystals have been proved to be excellent laser media for the 1.3 μm lasers. Among these laser media, the Nd:YAG crystal has played an important role in 1.3 μm laser generation [1, 2]. Subsequently, Nd-doped vanadate crystals are also alternatives in this spectral range [3–5]. Nd-doped disordered crystals process the inhomogeneous broadening and the spectral and thermal merits of both Nd-doped glass and ordered crystals. As a consequence, Nd-doped disordered crystals have attracted rising interest in recent years. In comparison with the most common garnet crystal Nd:YAG, along with the same space group structure and excellent physicochemical properties, the Nd:LGGG crystal also possesses a broad emission band owing to the more disordered structure induced by Lu^{3+} doping [6, 7]. Therefore, the Nd:LGGG crystal is considered to be a promising candidate for efficient lasing at 1.3 μm.

Shang Gao, Wei Wang School of Science, Shandong Jiaotong University, Jinan, 250357, China; e-mail: wwangsl@sdjtu.edu.cn

Received 8 September 2010; revision received 9 November 2020
Kvantovaya Elektronika **51** (2) 149–152 (2021)
Submitted in English

Passively *Q*-switched lasers can generate short duration pulses with a high peak power. Up to date, several saturable absorbers lasers, such as a Co^{2+}:LMA crystal [8, 9], semiconductor saturable absorber mirror (SESAM) [10], V:YAG crystal [3–5, 9, 11] and other nanomaterials [12–16], have been employed for *Q*-switched 1.3 μm. Experimentally, the pulse duration of the *Q*-switched lasers with Co^{2+}:LMA is relative large, which results in a low peak power. While the use of SESAM requires elaborate design and complicated fabrication, which limits its applications. The low-dimensional nanomaterials suffer from the long-term stability. In comparison with other saturable absorbers, the V:YAG crystal is an excellent saturable absorber for 1.3 μm lasers owing to its excellent physical and optical properties, such as large ground-state absorption cross section ($\sigma_g = 7.2 \times 10^{-18}$ cm^2), low saturable energy density (~0.05 J cm^{-2}), high damage threshold, and low residual absorption at 1.3 μm [17]. In 2012, S. Liu et al. reported a passively *Q*-switched Nd:LGGG with a V:YAG saturable absorber at 1330 nm [18]. However, some important characteristics of an Nd:LGGG laser based on the $^4F_{3/2} \rightarrow {}^4I_{13/2}$ transition of a neodymium ion, such as lasing spectra, thermal optical coefficient and tunable range, have not been reported yet.

In this paper, the laser performance in cw and passively *Q*-switching regimes were investigated in detail.

2. Experimental setup

The experimental setup of the cw and passively *Q*-switched Nd:LGGG lasers is shown in Fig. 1. The pump source was a fibre-coupled laser-diode (FAP-I system, Coherent Inc., USA) with a centre wavelength at 808 nm. The pump beam was collimated and focused into the Nd:LGGG crystal with a spot of 400 μm in diameter by an optical system. The Nd:LGGG crystal was grown by Chokhralski method and had a Nd-dopant of 1 at. %. The ⟨111⟩-cut Nd:LGGG measuring $4 \times 4 \times 3.8$ mm was wrapped with a thin layer of indium foil and mounted in a copper holder to maintain at 18 °C. The resonator was a conventional plane-concave cavity formed by a concave mirror M1 [a radius of curvature (ROC) of 200 mm, a high-reflectivity (HR) coating at 1330 nm ($R >$ 99.5%) and a high transmission (HT) coating at 808 and 1064 nm ($T = 90\%$)] and an output coupler (OC) [a plane mirror with a transmission $T = 5\%$ at 1330 nm and HT at 1064 nm ($T > 90\%$)] to suppress the 1064 nm oscillation. The V:YAG crystal [anti-reflectivity (AR) coated at 1330 nm, $R < 0.2\%$] with a small signal transmission of 90% was employed as a passive *Q*-switch. The total laser cavity length was approximately 25 mm. A MAX 500AD laser power meter (Coherent Inc., USA), a DPO 7104C digital phosphor oscil-

loscope (1 GHz bandwidth and 20 GHz sampling rate, Tektronix Inc., USA), a fast InGaAs photodetector (rising time of about 0.4 ns, New Focus 1611) and a Wavescan Laser spectrometer (0.5 nm resolution, APE GmbH, Germany) were employed to measure the output power and the spectra of the laser, respectively.

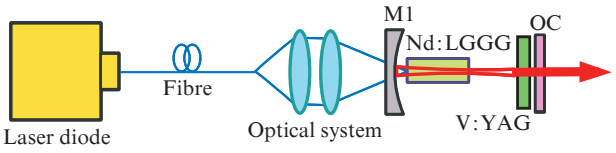

Figure 1. Schematic of the setup for studying Nd:LGGG lasing characteristics based on the $^4F_{3/2} \rightarrow {}^4I_{13/2}$ transition of a neodymium ion.

3. Results and discussions

Figure 2 depicts the average output power versus the incident pump power. The threshold incident pump powers for cw and *Q*-switching regimes are about 0.82 W and 3.41 W, respectively. In the cw regime, a maximum output power of 802 mW was obtained at an incident pump power of 7.09 W, corresponding to a slope efficiency of 13.2%. In the *Q*-switching regime, a maximum output power was 176 mW. It is worthy to note that the output power for the cw regime decreased when the incident pump power was higher than 7.09 W. The possible reason can be attributed to the serious thermal lensing effect in the Nd:LGGG crystal. It is well known that the thermal lensing effect at 1.3 μm is much graver than that at 1.06 μm due to the larger quantum defect as well as strong excited state absorption (ESA) for 1.3 μm.

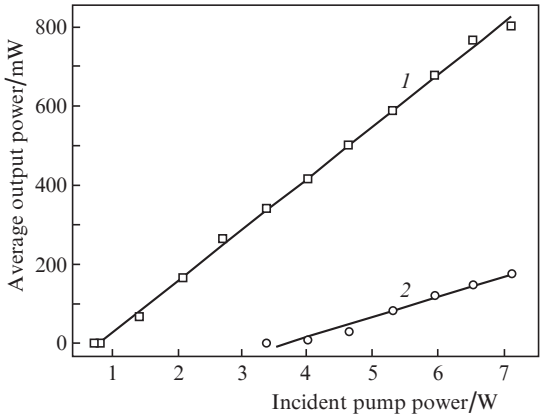

Figure 2. Average output power in the cw regime [η = 13.2% (*1*)] and *Q*-switching regime [η = 5.1% (*2*)] vs. the incident pump power.

Since the output power decreased at a pump power exceeding 7.09 W, we assumed the laser resonator became unstable when the pump power was beyond this pump level owing the thermal lensing effect of the gain medium. By using the conventional ABCD matrix method, the focal length induced by the gain medium at a pump power of 7.09 W was estimated to be about 26 mm. The focal distance of the thermal lens is related to the incident pump power P_{in} by the expression [19, 20]:

$$f = \frac{\pi K_c w_p^2}{\xi P_{in}(dn/dT)[1 - \exp(-\alpha l)]}, \quad (1)$$

where K_c = 9.66 W mK^{-1} [7] is the thermal conductivity of the crystal, w_p is the average beam radius of the pump light in Nd:LGGG, ξ is the thermal load fraction (~39.3%), α = 5.76 cm^{-1} is the measured absorption coefficient, and l is the length of the Nd:LGGG crystal. Therefore, the thermal optical coefficient (dn/dT) for the Nd:LGGG crystal at 1.33 μm was estimated to be about 15.3 × 10^{-6} K^{-1}, which is in agreement with the Nd:GGG crystal (16.4 × 10^{-6} K^{-1}) [21].

Under the threshold pump power of 0.82 W, the corresponding thermal focal length was about 224 mm, while the beam waist w_c in the laser cavity was estimated to be 136 μm. The threshold pump power in the cw regime can be expressed as [22]:

$$P_{th} = \frac{\pi h\nu_p(w_p^2 + w_c^2)(T + L)}{4\eta_p \sigma\tau}, \quad (2)$$

where $h\nu_p$ is the pump photon energy, η_p = 1 is the excitation quantum efficiency, L is the intrinsic losses in the cavity, σ is the stimulated emission cross section, τ = 243 μs is the excited state fluorescence lifetime [7], and T is the effective output coupling of the cavity by taking the absence of the coatings on the crystal faces. The stimulated emission cross section was estimated to be about 4.2 × 10^{-20} cm^2, in agreement with Ref. [18].

The lasing spectra were investigated in detail. Figure 3 shows several typical spectra at different incident pump powers. In the cw regime, the FWHM of the lasing spectra became broader with an increase in the incident pump power, indicating more and more modes oscillated in the laser cavity. When the small-signal gain was larger than the losses, the laser could oscillate in a resonator. The small-signal gain depended on the population densities of laser levels, which was determined by the pump intensities. As shown in Fig. 3a, the wavelengths near 1335 and 1323 nm can operate with the enhancement of the incident pump power. In the *Q*-switching regime, the peaks of the spectra are centred near 1331.3 nm. It is interesting that dual-wavelength operation at 1331.2 and 1335.2 nm could be observed under an incident pump power of 7.09 W,

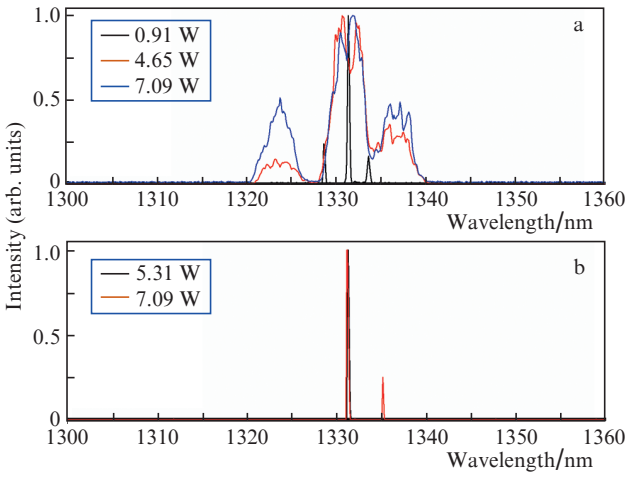

Figure 3. (Colour online) Typical lasing spectra in (a) cw and (b) *Q*-switching regimes at different incident pump powers.

as shown in Fig. 3b. Further optimising the laser resonator, balanced dual-wavelength operation with a high peak power could be used to obtain Thz radiation by using difference frequency generation (DFG) technology. As shown in Fig. 3a, the FWHM of the lasing spectra was very broad, which may be used to obtain ultrashort pulses.

For the passively Q-switched Nd:LGGG laser with a V:YAG saturable absorber, the dependences of the pulse duration and the pulse repetition rate on the incident pump power are shown in Fig. 4. One can see that the pulse duration decreases with increasing incident pump power. A minimum pulse duration of 9.75 ns was obtained under an incident pump power of 7.09 W. While the pulse repetition rate increased with the incident pump power. The highest pulse repetition rate was 8 kHz.

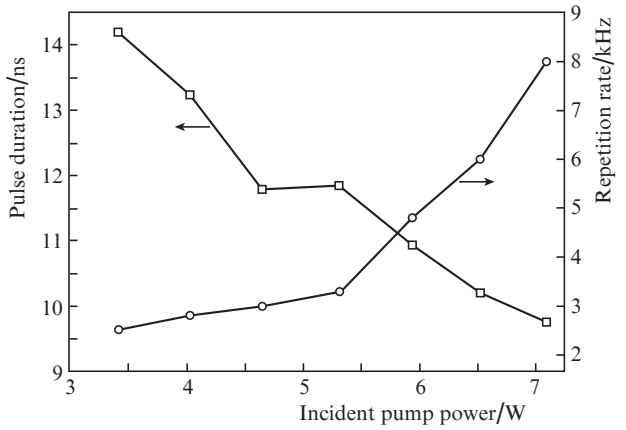

Figure 4. Pulse duration and pulse repetition rate vs. the incident pump power.

The pulse energy and the peak power can be calculated by using the estimated output power, pulse duration and pulse repetition rate. Figure 5 shows the dependence of the pulse energy and the peak power on the incident pump power. The maximum pulse energy and the highest peak power were about 25.4 μJ and 2.4 kW, respectively. Figure 6 illustrates typical oscilloscope traces, demonstrating a stable operation of the laser in the Q-switching regime. One can see that at

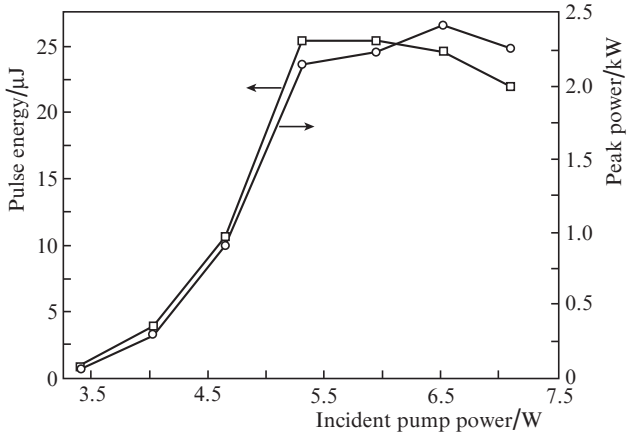

Figure 5. Pulse energy and peak power vs. the incident pump power.

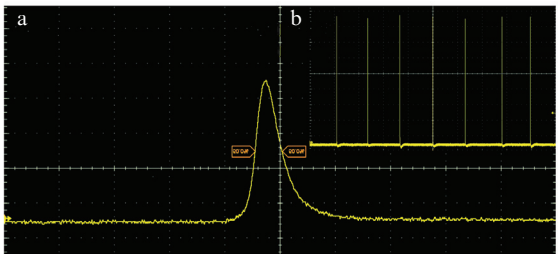

Figure 6. Typical oscilloscope traces under an incident pump power of 7.09 W: (a) temporal pulse shape with a FWHM duration of 9.75 ns and (b) a stable pulse train with a pulse repetition rate of 8 kHz.

P_{in} = 7.09 W ns a stable pulse train with a duation of 9.75 ns and a pulse repetition rate of 8 kHz is generated.

A typical V-type resonator was utilised to tune the frequency of the Nd:LGGG laser based on the $^4F_{3/2} \rightarrow {}^4I_{13/2}$ transition of a neodymium ion. Use was also made of a folded mirror with a ROC of 200 mm and HR coating at 1330 nm ($R > 99.5\%$). The arm lengths were 155 and 245 mm. As a frequency filter, a 2 mm-thick quartz plate with its optical axis in the plane of the input face was inserted into the resonator tilted at the Brewster angle. The tuning range under an incident pump power of 7.09 W is shown in Fig, 7. The experimental results shown in Fig. 7 imply that the Nd:LGGG laser near 1331 nm can be used to generate ultrashort pulses.

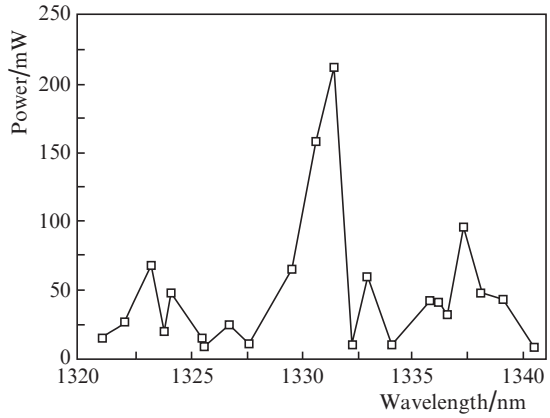

Figure 7. Tuning curve of the Nd:LGGG laser based on the $^4F_{3/2} \rightarrow {}^4I_{13/2}$ transition of an neodymium ion at P_{in} = 7.09 W.

4. Conclusions

Laser characteristics of a disordered mixed Nd:LGGG laser based on the $^4F_{3/2} \rightarrow {}^4I_{13/2}$ transition of a neodymium ion were investigated. In the cw regime, a maximum output power of 802 mW was obtained with a slope efficiency of 13.2%. The thermal optical coefficient for the Nd:LGGG crystal at 1.33 μm was estimated to be 15.3×10^{-6} K^{-1}. In the Q-switching regime, a minimum pulse duration was 9.75 ns with a maximum output power of 176 mW and a highest pulse repetition rate of 8 kHz. Moreover, a dual-wavelength operation at 1331.2 and 1335.2 nm can be observed under an incident pump power of 7.09 W. By using a 2 mm-thick quartz plate as frequency filter, the laser frequency can be tuned.

Acknowledgements. This work is supported by the Shandong Provincial Natural Science Foundation of China (Grant Nos ZR2020MF102 and ZR2017MA040).

References

1. Liu L., Huxley J., Ippen E., Haus H. *Opt. Lett*., **15**, 553 (1990).
2. Hall G., Ferguson A. *Opt. Lett*., **19**, 557 (1994).
3. Liu F., He J., Zhang B., Xu J., Dong X., Yan K., Xia H., Zhang H. *Opt. Express*, **16**, 11759 (2008).
4. Yang K., Zhao S., He J., Zhang B., Zuo C., Li G., Li D., Li M. *Opt. Express*, **16**, 20176 (2008).
5. Huang H., Zhang B., He J., Yang J., Xu J., Yang X., Zuo C., Zhao S. *Opt. Express*, **17**, 69461 (2009).
6. Jia Z., Tao X., Yu H., Dong C., Zhang J., Zhang H., Wang Z., Jiang M. *Opt. Mater*., **31**, 3469 (2008).
7. Fu X., Jia Z., Li Y., Yuan D., Dong C., Tao X. *J. Cryst. Growth*, **353**, 726 (2012).
8. Huang H., He J., Zuo C., Zhang H., Wang J., Wang H. *Appl. Phys. B*, **89**, 319 (2007).
9. Cheng K., Zhao S., Li Y., Li G., Li D., Yang K., Zhang G., Li X. *J. Opt. Soc. Am. B*, **28**, 149 (2011).
10. Fluck R., Braun B., Gini E., Melchior H., Keller U. *Opt. Lett*., **22**, 991 (1997).
11. Li H., Zhang R., Tang Y., Wang S., Xu J., Zhang P., Zhao C., Hang Y., Zhang S. *Opt. Lett*., **38**, 4425 (2013).
12. Pan H., Cao L., Chu H., Wang Y., Zhao S., Li Y., Qi N., Sun Z., Jiang X., Wang R., Zhang H., Li D. *ACS Appl. Mater. Interfaces*, **11**, 48281 (2019).
13. Dong L., Li D., Pan H., Li Y., Zhao S., Li G., Chu H. *Appl. Opt*., **58**, 8194 (2019).
14. Chu H., Li Y., Wang C., Zhang H., Li D. *Nanophoton*., **9**, 761 (2020).
15. Dong L., Huang W., Chu H., Li Y., Wang Y., Zhao S., Li G., Zhang H., Li D. *Opt. Laser Technol*., **128**, 106219 (2020).
16. Ca L., Chu H., Pan H., Wang R., Li Y., Zhao S., Li D., Zhang H., Li D. *Opt. Express*, **28**, 31799 (2020).
17. Malyarevich A., Denisov I., Yumashev K., Mikhailov V., Conroy R., Sinclair B. *Appl. Phys. B*, **67**, 555 (1998).
18. Liu S., Jia Z., He J., Zhang B., Yang X., Liu F., Xu J., Tao X. *IEEE Photonics Technol. Lett*., **24**, 146 (2012).
19. Innocenzi M., Yura H., Fincher C., Fields R. *Appl. Phys. Lett*., **56**, 18313 (1990).
20. Chu H., Zhao S., Yang K., Zhao J., Li D., Li G., Li T., Qiao W., Xu X., Zheng L., Xu J. *Opt. Mater*., **45**, 181 (2015).
21. Wang Z., Huang L., Zhang Q., Zhang G., Sun D., Yin S. *J. Optoelectron. Laser*, **18**, 956 (2007) (in Chinese).
22. Jaque D., Capmany J., Sole J., Brenier A., Boulon G. *Appl. Phys. B*, **70**, 11 (2000).